Received: 6 May 2017 | Accepted: 7 August 2017

DOI: 10.1111/jace.15162

ORIGINAL ARTICLE

Journal of the American Ceramic Society

Porcelain stoneware consolidation by flash sintering

Mattia Biesuz[1] | **Woinshet D. Abate**[1] | **Vincenzo M. Sglavo**[1,2]

[1]Department of Industrial Engineering, University of Trento, Trento, Italy

[2]INSTM Research Unit, Firenze, Italy

Correspondence
Mattia Biesuz, Department of Industrial Engineering, University of Trento, Trento, Italy.
Email: mattia.biesuz@unitn.it

Abstract

Porcelain stoneware was consolidated by flash sintering under DC polarization using current densities in the range 4-20 mA/mm^2. The results show the applicability of this innovative sintering technology to a material whose densification occurs by vitrification, thus allowing to extend the possible application field of flash sintering to traditional ceramics. Using appropriate current density, the flash-sintered samples are dense, homogeneous, and well-vitrified. XRD and microstructural analysis points out the formation of primary mullite while secondary mullite is only sporadically observed. In addition, comparison between flash sintering and fast firing shows that the densification obtained in the selected ceramic system via the former route cannot be reproduced just by a rapid heating process.

KEYWORDS

field-assisted sintering technology, porcelain, sinter/sintering

1 | INTRODUCTION

Flash sintering (FS) is a very innovative and promising consolidation technology for producing ceramic components: it allows a drastic reduction in processing time and temperature,[1–3] thus leading to important reduction in equipment and energetic costs. FS belongs to the group of the so-called field-assisted sintering techniques but, when compared with other field-assisted processes like spark plasma sintering, it is definitely much simpler and cheaper, not requiring the use of sophisticated components or devices.

During flash sintering, the sample is connected to a power supply and, at a certain combination of electrical field and temperature, an abrupt decrease in electrical resistivity is observed, the material undergoing to a sort of transition from electrical insulator to conductor.[1,2,4] This phenomenon is followed by an intense light emission[1,5,6] and an almost instantaneous densification occurs in few seconds. Although the first FS experiments were carried out on ionic conductors (YSZ, GDC, etc.),[1,2,7–10] it is now clear that several advanced ceramics ranging from electrical conductors[11–13] to insulators[14,15] can be consolidated by flash sintering.

In 2015, McLaren et al. have shown a kind of flash event also on alkali-silicate glasses.[16] In such case, glass viscosity decreases abruptly upon heating under the application of an electrical field, this being accompanied by greater electrical conductivity and intense photoemission. This phenomenon takes place at temperatures far lower than those usually needed for glass softening, and for this reason, the process was called "electric field-induced softening".[16]

On these bases, in a recent work, we have shown that flash sintering can be applied to ceramic systems containing some glassy phase (magnesia silicate glass-containing alumina).[17] The results indicated a very rapid and effective densification via liquid phase sintering at quite moderate temperatures, suggesting that viscous properties of glass are influenced by current flow.

The purpose of the present work is to expand the possible application field of flash sintering to traditional ceramics, which represent a large portion of the ceramics market, and in particular to porcelain stoneware, typically used for the production of tiles. Such ceramic material is characterized by complex consolidation process where raw materials form abundant high viscosity glassy phase which promotes vitrification,[18] densification occurring via viscous flow sintering mechanisms[19] at temperatures typically from 1200 and 1300°C[20] depending on raw materials composition.

The goal here is to analyze how glassy phase formation and successive consolidation are influenced by the application of an external electrical field in a typical industrial porcelain stoneware composition.

2 | EXPERIMENTAL PROCEDURES

Commercially available porcelain stoneware raw material was used in this work. The nominal composition is 43-49 wt% clays, 23-28 wt% sodium feldspar, 8-11 w% potassium feldspar, and 13-18 wt% quartz. X-ray diffraction analysis (XRD) pointed out that clays are mainly constituted of kaolinite and feldspars (albite [$NaAlSi_3O_8$] and anorthoclase [$(Na,K)(Si_3Al)O_8$].

A preliminary characterization of the raw materials was carried out by thermogravimetric/thermodifferential analysis (TGA/DTA) and dilatometric tests. TGA/DTA was carried out at 20°C/minutes up to 1200°C in a Netzsch STA 409 instrument using alumina as a reference. The dilatometric test was performed using a cylindrical pellet (diameter≈13 mm), produced by uniaxial pressing at 120 MPa; a Linseis L75 dilatometer was used with heating rate of 20°C/minutes and applied load of 500 mN.

Dog bone-like samples were produced by uniaxial pressing at 120 MPa for flash sintering experiments. The sample geometry was similar to that reported in a previous work,[15] the cross section of the central part of the gage section being 3.0 mm by 1.4-1.8 mm; the length of the gage section was 20 mm. The bulk density of green bodies after drying (120°C, 2 hour) was about 1.90-1.92 g/cm^3 (measured using a digital balance and caliper with sensitivity equal to ±0.0001 g and 0.01 mm, respectively).

The samples were presintered at 950°C in a muffle furnace under static air for 60 minutes; the heating rate was 10°C/minutes while the samples were let to cool down freely within the furnace. Presintering was carried out to improve the mechanical strength of the specimens and facilitate their manipulation. In addition, since flash experiments were performed by introducing the specimens in a preheated furnace, presintering allowed a preliminary decomposition of kaolin, thus avoiding sudden water evolution which could damage the material. After presintering, the bulk density of the specimens was about 1.87-1.89 g/cm^3, which confirms the absence of any densification effects.

The presintered specimens were connected by two platinum wires to a DC power supply (Glassman EW series 5 kV-120 mA) and to digital a multimeter (Keithley 2100). The ceramic/metal connection was obtained by forcing the platinum wires within the holes present on the opposite sides of the dog bone. Then, the specimens were introduced in the center of a preheated tubular furnace (Nabertherm P330) and, after 1 minute, the power supply was switched on. After the current limit was reached, the system was let to work under current control for 30 seconds; then, the power supply was shutdown and the sample was suddenly removed from the furnace.

The main part of the flash sintering experiments reported in this work were carried out at a furnace temperature of 1000°C and voltage limit of 1750 V/cm. In order to point out the current density effect on densification, the specimens were subjected to flash sintering using different current limit in the range 4-20 mA/mm^2 and dwell time of 30 seconds. In addition, the combination of onset field-temperature for reproducing the flash event was investigated. In this case, the voltage limit was progressively reduced (by 50 V/cm each test) until the flash event was no more observed (test duration = 5 min). The onset field for FS was determined for different furnace temperatures from 900 to 1050°C.

In order to point out the current flow effect on densification, some samples were subjected to fast firing. Thinner samples (~1.1 mm) were produced and presintered (following the same thermal cycle used for specimens subjected to FS) to reduce their thermal capacity and allow a rapid heating process. Fast firing was carried out in a tubular furnace (Nabertherm P330) preheated at different temperatures (1100-1500°C). The samples were directly introduced into the furnace[21] and left there for 45 seconds. Treating time was 15 seconds longer than that used during FS because the specimens needed some time to reach equilibrium with furnace temperature. This time lag can be estimated using the following approximations: all the heat is exchanged by radiation, the sample temperature is homogeneous and the material thermal capacity is 1000 J/kg K.[22] Assuming that the total emissivity to be 0.93,[23] the time needed for the sample to reach the furnace temperature (ΔT < 3°C) can be estimated in the order of 8 second or less (for details see Appendix 1). Even assuming a lower emissivity, i.e., 0.8, this time lag is lower than 10 seconds. Some extra seconds were added in the fast firing experiments for improving temperature homogeneity.

The density of sintered specimens was measured by the Archimedes method using an analytical balance (Gibertini, sensitivity = ±0.0001 g): only the constant cross-section portion of the dog bone samples was considered and measurements were repeated on two different samples for each processing conditions.

Finally, the microstructure and phase distribution was studied by SEM (Jeol JSM 5500) and EDS (JEOL IXRF SYSTEMS 500, using the software Iridium Ultra). Micrographs were taken on the external surface of the flash-sintered samples; in some cases, the surface was carefully polished using diamond pastes and chemically etched for 30 seconds in 5 vol% HF-containing water solution.

Mineralogical analysis was carried out on monolithic sintered bodies using a IPD3000 diffractometer and Cu Kα as a X-ray source (exited with 30 mA-40 kV). The spectra were collected by means of an Inel CPS120 detector for 15 minutes.

3 | RESULTS AND DISCUSSION

3.1 | Preliminary characterization of the raw material

TG/DTA and dilatometric plots of the raw material used in the present work are reported in Figure 1. The weight loss upon heating is equal to 7.1 wt% and corresponds to two main events, both associated with endothermic events: the first one (<0.5 wt%) occurs at ~80-100°C and corresponds to the evaporation of absorbed water and the second one starts at about 500°C and is associated to the dehydroxilation of kaolin, which evolves into metakaolin. This latter weight loss equal to ~7 wt% is coherent with the mineralogical composition of the raw material: as a matter of fact, the theoretical weight loss for kaolin-to-metakaolin transformation is equal to 14 wt% and the kaolin load in the used powder is close to 50 wt%.

DTA plot shows the presence of an exothermic reaction also at ~990°C, associated with the formation of Al-Si spinel/mullite and glass from metakaolin.[18,24–26]

Also, the dilatometric plot (Figure 1B) is very similar to those reported for porcelain in many ceramics textbook[27] and it shows three fundamental shrinkage events. The first one, at about 590°C, is related to kaolin decomposition; the second one is very likely due to the formation of Al-Si spinel/mullite and glass from metakaolin; and the third event, which is associated to ~10% shrinkage and which typically corresponds to real densification, reaches a maximum rate at 1190°C and it is associated to viscous flow sintering mechanisms. The material continues to shrink up to 1290°C and then it starts expanding. This behavior is well-known in porcelain production[28,29] and it is related to the formation of molecular oxygen in the glassy phase because of the oxidation state variation of some metallic ions (like iron); in addition, the volume increase can be accounted by the expansion of air entrapped within closed pores in the evolving glassy phase.

3.2 | Flash sintering of porcelain stoneware and microstructural evolution

The nominal electric power dissipated in porcelain upon flash sintering is reported in Figure 2 (furnace temperature = 1000°C). One can observe that the material undergoes to the typical behavior usually observed in FS experiments. In fact, initially, the electrical conductivity of the ceramic increases slowly, causing an intensification of the specific power dissipation. Then, the flash event takes place; it is characterized by an abrupt drop of electrical resistivity associated to the power peaks in the diagrams of Figure 2. After such phenomenon, the power supply starts to work in current control and the electrical power stabilizes. The time needed for reproducing this sort of transition from insulator to semiconductor-like, called incubation time, clearly depends on the applied field: the samples treated at higher electrical filed are characterized by shorter incubation times, this being similar to the behavior shown by other crystalline ceramics.[4,30]

The minimum field (sensitivity = 50 V/cm) needed for triggering the flash event at different furnace temperatures is reported in Table 1. One can observe that such threshold field strength, in the range 350-500 V/cm, decreases with furnace temperature. If a more intense field is applied, flash sintering can be successfully reproduced in porcelain; conversely, if the field is lower, the material does not undergo to flash sintering. Such relationship between onset E-field and furnace temperature was observed in many crystalline ceramics and finds solid bases in the model for thermal runaway for flash sintering.[31–35]

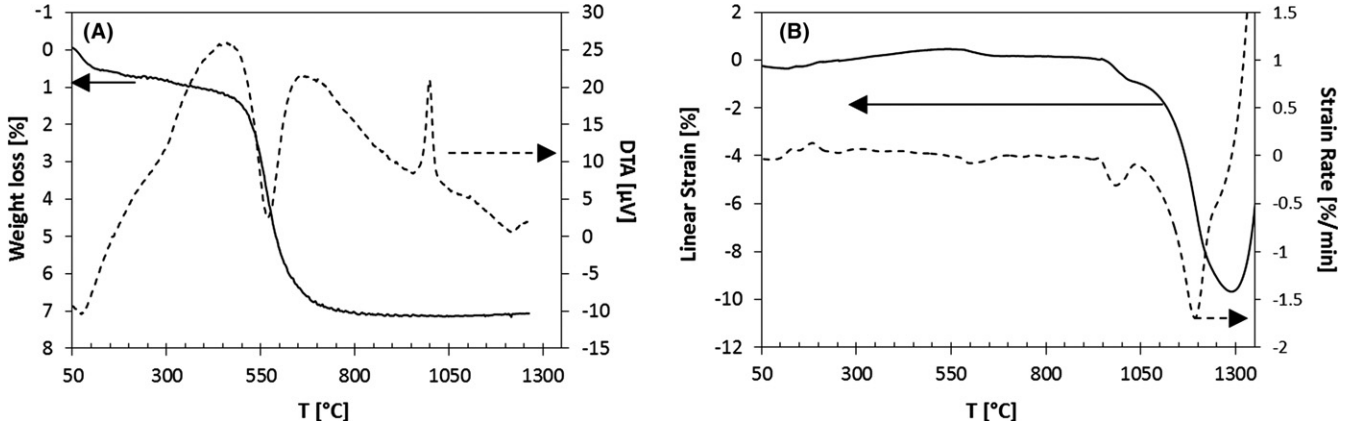

FIGURE 1 (A) TGA/DTA plot recorded on the raw powder; (B) dilatometric strain and linear strain rate measured on porcelain green pellet

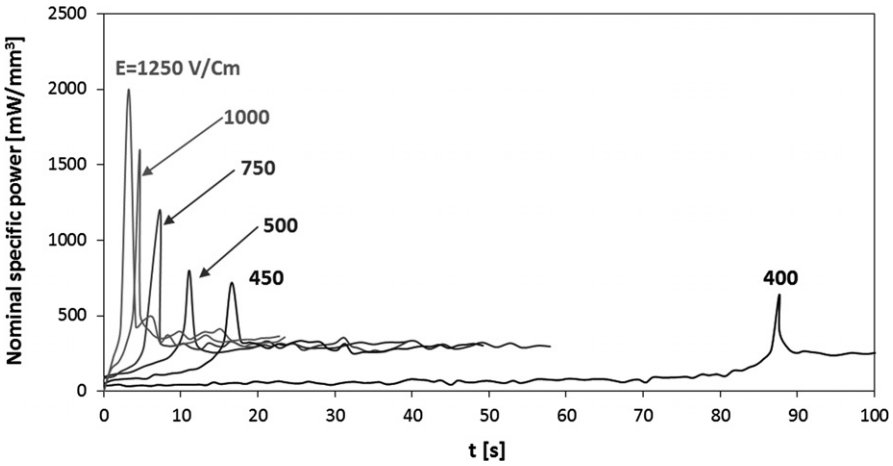

FIGURE 2 Electrical power dissipation in ceramic specimens upon flash sintering experiments at 1000°C (current limit = 16 mA/mm^2)

TABLE 1 Onset conditions for flash sintering

Furnace temperature [°C]	Onset field for flash sintering [V/cm]
900	500
950	450
1000	400
1050	350

The microstructural evolution of samples flash sintered at 1000°C for 30 second with different current limits is shown in Figure 3A. The micrographs were taken on the external surface of the samples in the central part of the gage section. One can observe that the material becomes progressively denser by increasing the applied current, especially up to 14 mA/mm^2; for larger current densities, complete densification is achieved although furnace temperature and processing times are much lower than corresponding parameters used in conventional sintering treatments. Moreover, the low magnification micrographs in Figure 3B point out that the microstructure is well homogeneous in the constant cross-section area of the dog bone.

Interestingly, if current density in excess to 18 mA/mm^2 is used, some pores grow abnormally (reaching also tens of microns in diameter) and open on to the surface. This behavior is very likely related to mechanisms similar to those described in the previous section for the expansion revealed in the last portion of the dilatometric plot (Figure 1B).[28,29]

An additional fascinating aspect regards the surface smoothening which progressively increases with the applied current as shown in Figure 3; this is a clear indication that vitrification process becomes more and more intense, the glassy phase gradually dissolving the crystalline constituents.

XRD spectra collected on flash-sintered specimens and shown in Figure 4 point out a clear evolution of the crystalline phases with the imposed current limit: at very limited current (4 mA/mm^2), feldspars are still present while mullite is very limited; at 8 and 12 mA/mm^2, albite and anorthoclase substantially disappear, while the amount of mullite increases; at the highest current densities, only mullite and quartz are present, very likely incorporated within an abundant glassy phase matrix.

Additional details regarding the microstructure of flash-sintered samples can be collected by the observation under SEM of their surface after careful polishing and HF etching. Porosity evolution is clear on SEM pictures taken on polished surfaces (Figure 5): at limited current density, pores are small, copious, sharp, and sometimes elongated while for larger current values they become progressively more regular, larger with rounded shape, this indicating that they are surrounded by an isotropic, continuous vitreous phase. The comparison of micrographs in Figure 6 and XRD spectra (Figure 4) confirms that when feldspars dissolution and vitrification are substantially completed (using current limit of 12 mA/mm^2), and pores assume a spherical shape.

HF-etched sample micrographs are reported in Figure 6. The different phases can be identified according to EDS and XRD analysis results: quartz crystals are always present and correspond to relatively dark and smooth areas. At low current (4 mA/mm^2), the presence of kaolin decomposition products can be observed and feldspars are only partially decomposed. By increasing the current (12-20 mA/mm^2), both feldspars and kaolin are dissolved and only mullite and glass are visible.

Mullite crystals observed at higher magnification (Figure 7A and C) shows the microstructural features of typical primary mullite. This is formed in pure clay relicts and it is characterized by a very low aspect ratio (typically 1-3:1).[18,36] Generally, a second type of mullite, secondary mullite, can be formed in porcelain; it consists of needle-like crystals (aspect ratio in the range 3-40:1) with size that

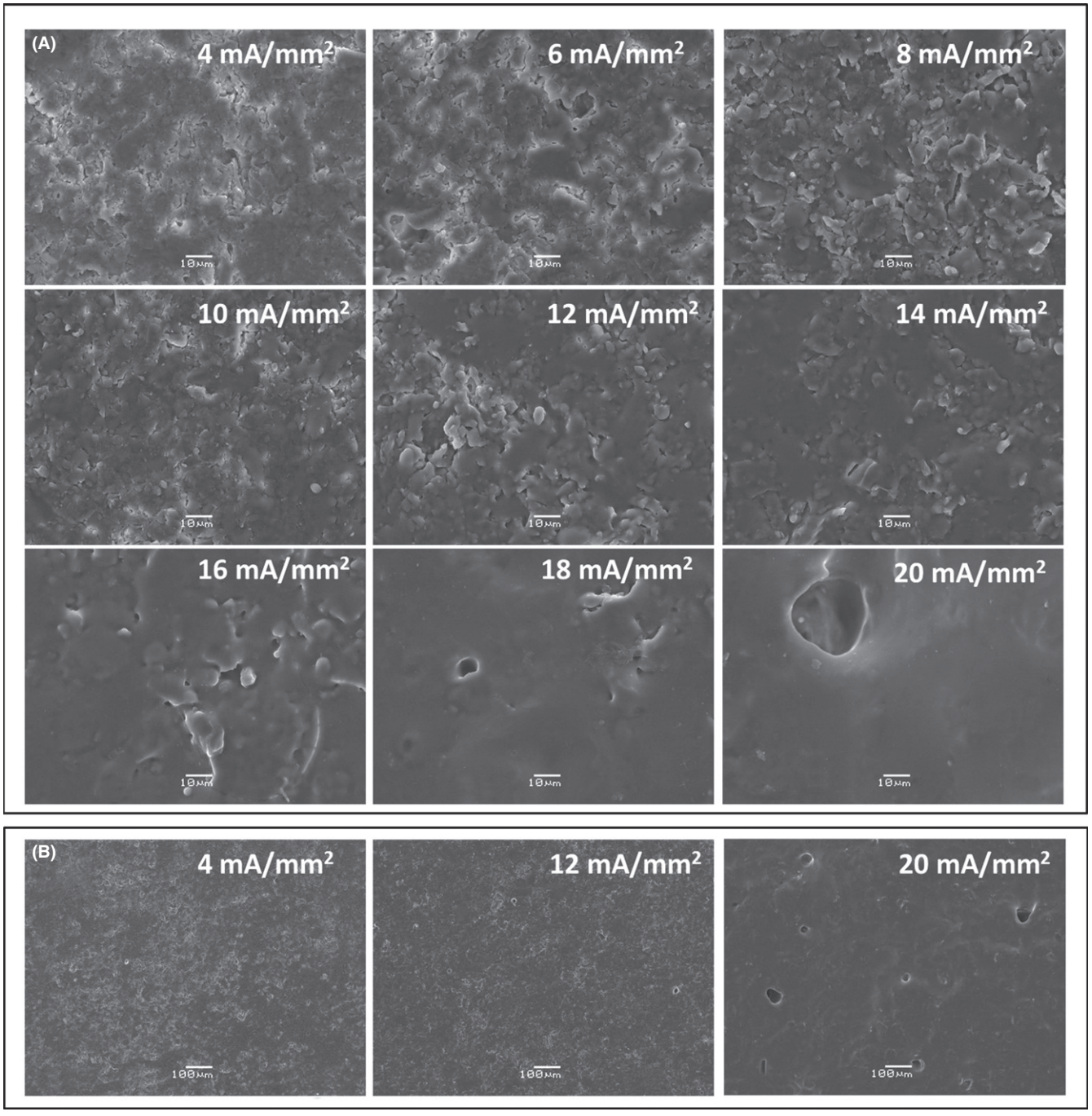

FIGURE 3 SEM micrographs at high (A) and low magnification (B) of the external surface of samples flash sintered using different current limit (furnace temperature = 1000°C)

can reach several microns.[36] Such kind of mullite is typically observed in feldspars relicts and it is formed by the reaction between the feldspars and the clays. In the present work, this kind of mullite can be only sporadically observed both in fast-fired and flash-sintered specimens. Some micrographs pointing out the formation of such crystals are reported in Figure 7B and D, the presence of secondary mullite being in any case local and restricted to small areas.

3.3 | Densification upon flash sintering

Bulk density and open porosity measured on flash-sintered and fast-fired samples are reported in Figure 8 as function of applied current and of firing temperature, respectively. The data in Figure 8 correspond to the average of two series of samples, the differences between the measurements being always lower than 0.07 g/cm^3 and 2.5% for bulk density and apparent porosity, respectively. Density

increases with current limit up to 14 mA/mm^2 for flash-sintered specimens, this being related to the glassy phase formation, which activates viscous flow sintering. In addition, the equilibrium sample temperature during flash sintering increases with applied current and this reduces the glass viscosity and promotes densification. Nevertheless, starting form 16 mA/mm^2, but becoming more significant at 18 mA/mm^2, swelling takes place and density decreases. Such effect is consistent with SEM observations discussed in the previous section, pointing out the formation of many large pores in samples treated with high currents. The highest density obtained by flash sintering is 2.45 g/cm^3, which well compares with density of conventionally sintered porcelain stoneware.[20] The swelling effect is less evident when open porosity is considered, it increasing weakly from 14 to 20 mA/mm^2. In such case, the expansion is due to the gas pressure increase within the closed pores and involves only marginally open porosity.

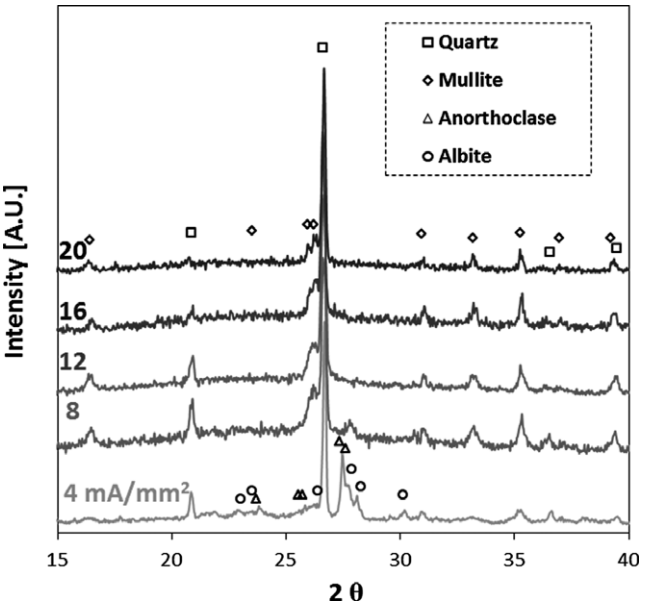

FIGURE 4 XRD spectra recorded on specimens flash sintered using different current limit (furnace temperature = 1000°C)

As for the fast-fired samples, the highest density (2.31 g/cm^3) is obtained for treatment at 1250°C. By increasing the furnace temperature, the density weakly decreases up to 1400°C; further increase in the firing temperature leads to an abrupt drop in porcelain density. It is worth to point out that the measured density after fast firing is in quite good agreement with the dilatometric plot (Figure 1B), which pointed out a material expansion at about 1290°C.

A comparison between flash-sintered and fast-fired materials is not straightforward. The two processes are clearly different the heat being generated internally in the former and absorbed from outside in the latter. In addition, it is difficult to estimate the real sample temperature during flash sintering. Nevertheless, both processes are

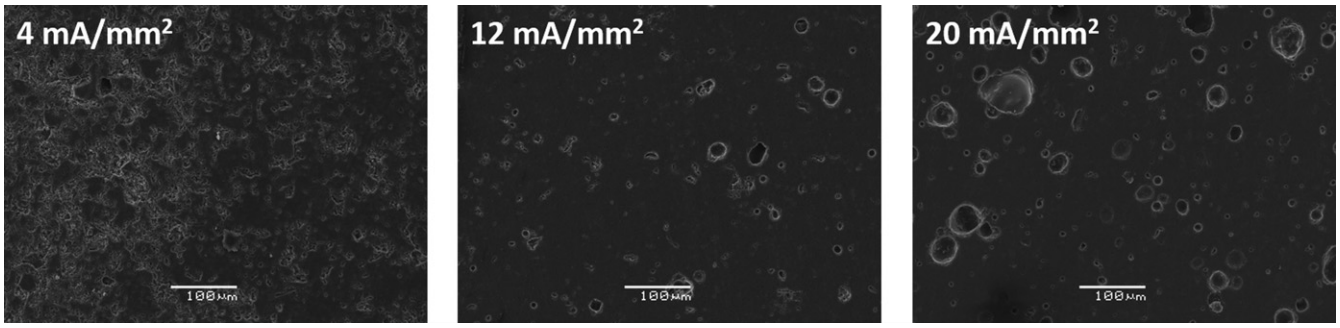

FIGURE 5 SEM micrographs of polished specimen flash sintered at 1000°C for 30 seconds

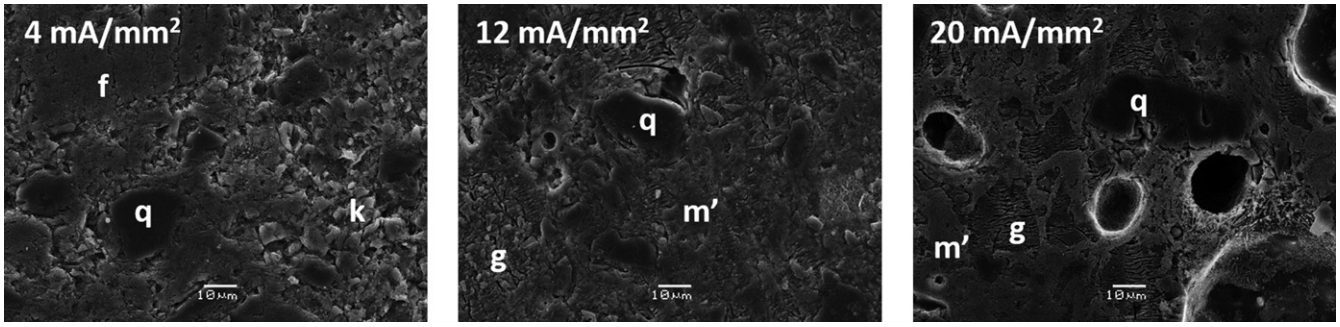

FIGURE 6 SEM micrographs of polished/etched specimen flash sintered at 1000°C for 30 second. The different phases: feldspars (f), kaolin relicts (k), quartz (q), glass (g), and primary mullite (m') are indicated

characterized by very rapid heating and limited times. In any case, data in Figure 7 point out that the maximum density achieved by the two processes is pretty different, 2.44 and 2.31 g/cm^3 for flash sintering and fast firing, respectively. Moreover, the limited open porosity in samples flash sintered using relatively high current density (1.1%) is not reproduced by fast firing even for treatments up to 1500°C (2.2%). This allows to hypothesize that densification phenomena upon flash sintering cannot be reproduced just by rapid heating.

In order to make the comparison between flash-sintered and fast-fired materials clearer, the specimen temperature (T_S) during the former treatment is needed. Its measurement is practically impossible using the experimental setup used in the present work. Therefore, it is estimated under the following assumptions: (i) the sample temperature is homogenous, (ii) the heat is completely exchanged by radiation, (iii) the geometrical parameters can be approximated with those measured on the sintered specimens, and (iv) the heat is dissipated only in the gage section.

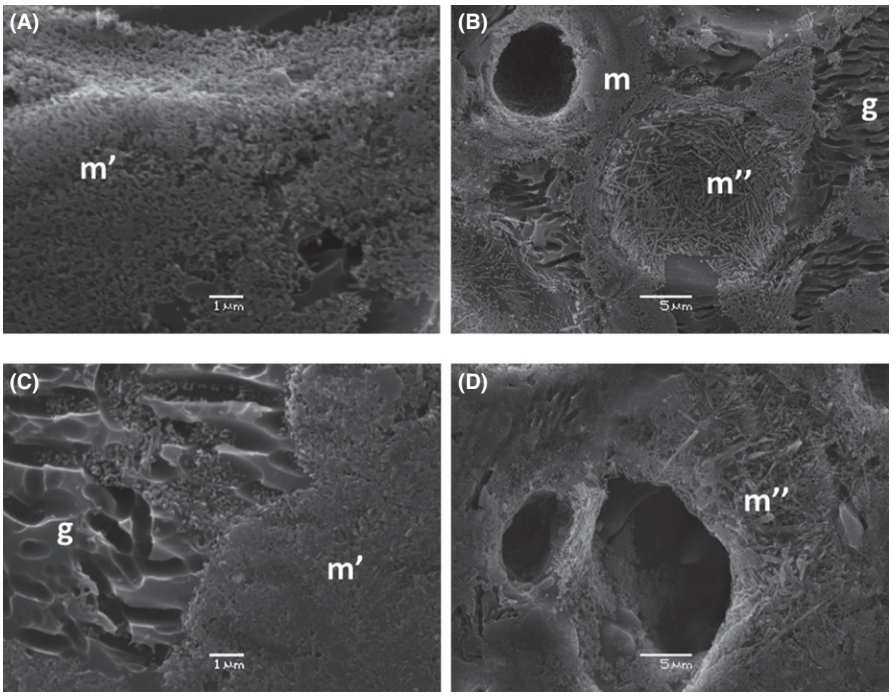

FIGURE 7 SEM micrographs of polished/etched (5% HF, 30 seconds) specimen treated by flash sintering using 20 mA/mm^2 (A,B) or by fast firing at 1400°C (C,D). The different phases: quarts (q), glass (g), primary (m'), and secondary mullite (m'') are indicated

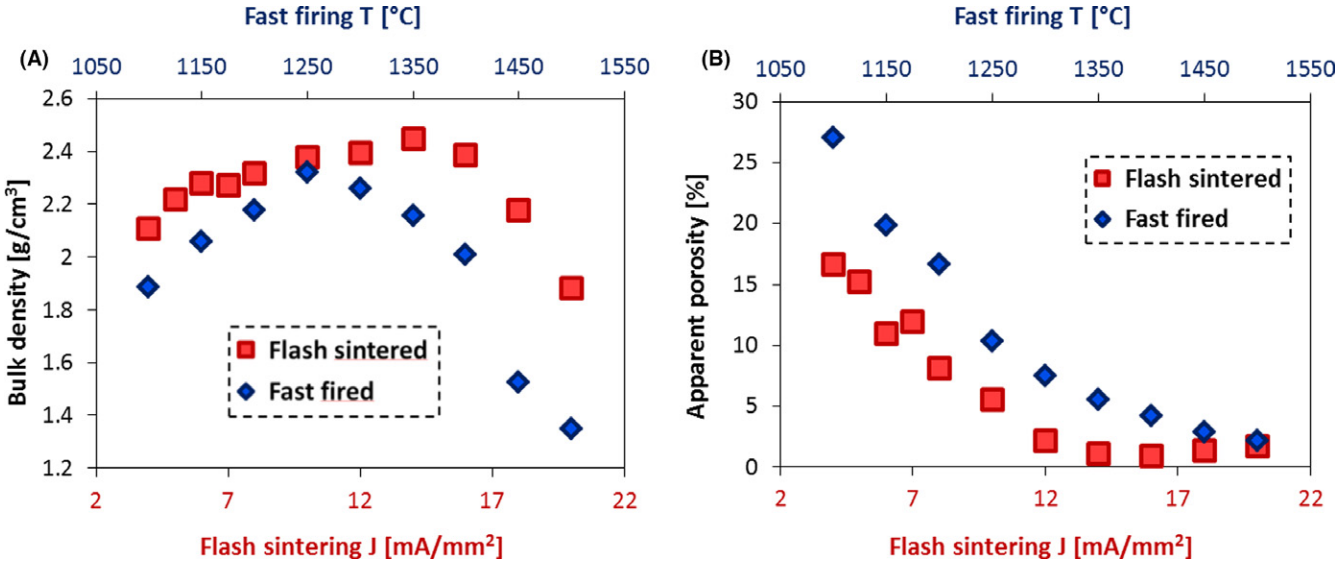

FIGURE 8 Bulk density (A) and open porosity (B) of flash-sintered and fast-fired specimens as function of current limit and furnace temperature. The two horizontal axes are not correlated [Color figure can be viewed at wileyonlinelibrary.com]

In order to ensure that the sample reaches equilibrium, only the data recorded starting 15 seconds after the flash event are considered. Under the reported assumptions, the power balance allows to write[37,38]:

$$T_S = \left(\frac{W_e}{S\sigma\varepsilon + T_F^4}\right)^{0.25} \quad (1)$$

where W_E is the electrical power, S the specimen surface area, σ the Stefan-Boltzmann constant, ε the emissivity, and T_F the furnace temperature. The emissivity is assumed to be 0.93 (according to data reported in the literature[23]). The sample temperature can be calculated also assuming a lower value of ε (0.8) in order to account of possible deviations from the reported emissivity. The gage section surface area was considered for S, it being the portion of the specimen where the electrical power is dissipated.

Once the temperature of the sample under flash sintering is known, bulk density and open porosity data can be plotted as shown in Figure 9. The maximum density for flash-sintered material is obtained when the estimated sample temperature is between 1240°C and 1295°C: this is in quite good agreement with the temperature at which the highest density was obtained in fast firing experiments. Moreover, we can observe that, below a certain temperature, the flash-sintered specimens are denser; conversely, if the sample temperature exceeds a certain value, fast-fired samples are the densest. Such transition is located at ~1305°C (ε = 0.93), only few degrees above the temperature where swelling starts, regardless the chosen emissivity values.

The interpretation of the densification differences in flash-sintered and fast-fired samples is a challenging task. The results reported in the scientific literature are somehow controversial. Some field/current-induced effects are claimed by some authors to explain rapid sintering in 3YSZ,[37] magnesia silicate glass-containing alumina,[17] and B_4C.[39] In other papers, it is suggested that the enhanced densification of 3YSZ and ZnO upon flash sintering shall be accounted for by an extremely high heating rate associated to the Joule effect[40,41]; such phenomenon was also associated to two distinct effects: (i) the rapid heating rate in crystalline ceramics often retarded grain coalescence with respect to densification thus allowing a fast densification of nanometric, highly sinterable powder; (ii) the grain-boundary structure obtained in a very rapid sintering process may differ from that at the equilibrium and may be characterized by unexpectedly high diffusion coefficients.[42] On the other hand, other authors suggested that the field application accelerates sintering by promoting the nucleation of lattice defects,[15] like Frenkel pairs, or by inducing grain-boundary overheating.[15] It is clear that such effects are unlikely to be observed in our work, the material being composed (during the sintering process) by a vitreous matrix with embedded quartz and mullite crystals. Therefore, the glass phase controls densification by viscous flows while crystalline grains, lattice defects or grain boundaries poorly affects sintering.

In order to explain the differences between flash-sintered and fast-fired samples, we can propose two possible physical models for the specific ceramic system, the former based on conventional theories and Joule heating, and the latter on the activation of field/current-induced phenomena. We want to point out that the two mechanisms are not applicable to crystalline ceramics like ZnO or 3YSZ whose densification upon flash sintering was suggested to be very similar to that achievable by a rapid heating without electric field and current.[40,41]

The first model regards the temperature evolution upon flash sintering, as a result of Joule heating; it can be better understood by analyzing the electrical behavior during the third stage of flash sintering. Figure 10 shows the nominal electric field (E) measured during the steady stage of flash sintering as a function of the nominal current density (J), the results referring to the last 15 second of the experiment

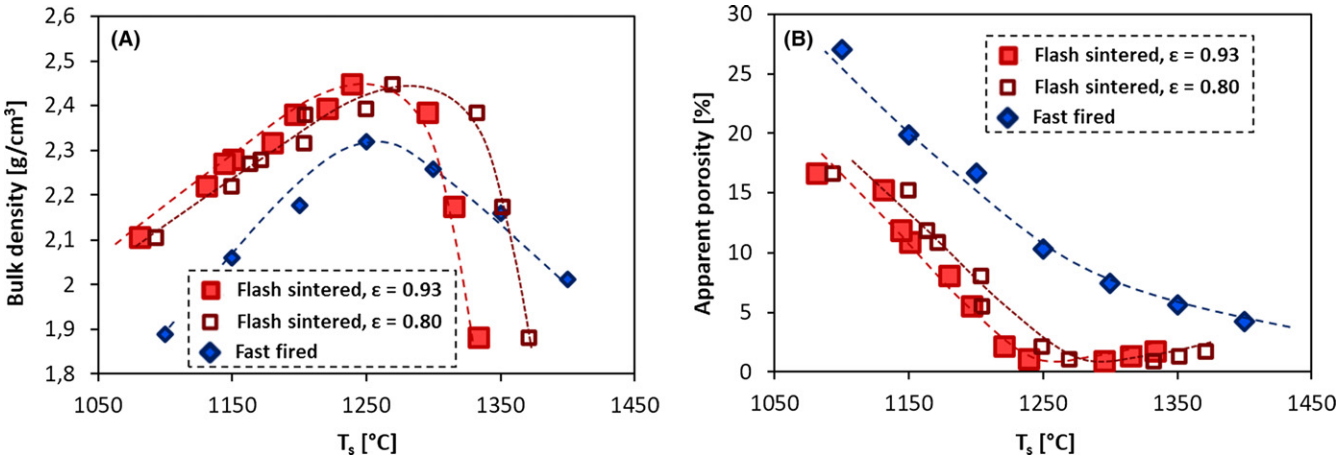

FIGURE 9 Bulk density (A) and open porosity (B) of flash-sintered and fast-fired specimens as function of the sample temperature. The temperature during flash sintering was estimated using emissivity equal to 0.93 and 0.8 [Color figure can be viewed at wileyonlinelibrary.com]

after E stabilizes. The relation is quite surprising: initially E decreases with J but, after reaching a minimum at 12 mA/mm^2, it stabilizes and slightly increases for larger current density.

It is well-known that the conductivity upon flash sintering depends on the current limit[14] and by increasing the applied current, the specimen becomes hotter and its resistivity (ρ) decreases. Since:

$$E = \rho J \tag{2}$$

the electrical field only slowly increases with J upon the flash state. Therefore, E/J relation reported in Figure 10, especially for J ≤ 12 mA/mm^2, is pretty unusual and different from previous findings on crystalline ceramic.[14]

As shown before in Figure 4, the vitrification process is not completed in the sample treated with current lower than 12 mA/mm^2; conversely, if larger currents are applied, glass is formed and no peaks related to feldspars can be observed. Therefore, we can assume that for limited currents the field decreases with J because of two effects: (i) the sample temperature increases with J and (ii) the amount of glassy phase progressively increases with J; in addition, since the produced glass contains large amount of alkaline ions (Na^+ and K^+) it should be quite conductive, decreasing the overall resistivity of the system. Nevertheless, when the current reaches 12 mA/mm^2, the vitreous phase is almost completely formed and E stabilizes. Now, we can imagine that, during the flash event, the temperature increases, this allowing a rapid glassy phase formation; but, once the glass is formed, the field strength decreases and this reduces the power dissipation and sample temperature as well. Therefore, when we calculate the equilibrium temperature during the steady stage of flash sintering, we cannot exclude a priori that before reaching the equilibrium the sample is hotter. This thermal evolution could lead to the formation of larger amount of glass than that expected at the equilibrium temperature. In this way, flash-sintered specimens are characterized by a more advanced densification than fast-fired ones, at least for temperatures lower than the swelling one.

This hypothesis is partially confirmed by XRD results. In fact, the peaks associated to feldspars disappear during flash sintering experiments between 8 and 12 mA/mm^2. In other words, considering the calculated sample temperature, this occurs between 1180 and 1220°C using ε = 0.93 (1200/1250°C for ε = 0.80). XRD spectra for such temperatures in fast-fired specimens (Figure 11) still show peaks associated with albite/anorthoclase; by increasing the firing temperature up to 1300°C, the peaks are still visible although with very limited intensity. It seems therefore that vitrification in flash-sintered specimen occurs at lower temperature when compared with fast-fired ones. Nevertheless, this could be the result of nonmonotonic temperature evolution during flash sintering, the sample temperature decreasing when the system is under current control, as a result of the glassy phase formation. In addition, if we assume that during the steady stage of flash sintering the sample core is hotter than the surface, this could also explain an accelerated swelling at high temperature. It has to be reminded anyway that Lebrun et al did not find evidences of temperature gradients in YSZ sample cross-section during the flash sintering steady stage.[43]

The second model proposed for explaining the plot in Figure 9 is based on the assumption that the current flow provides additional contribution to densification, which cannot be explained in terms of Joule heating, only. In particular, we can argue that the current flow changes the rheological properties of the glass responsible for viscous flow sintering. This could also explain some experimental

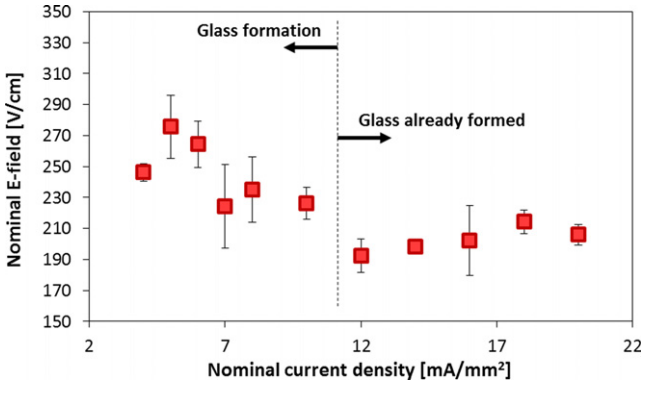

FIGURE 10 Electric field measured during the steady stage of flash sintering as a function of current limit (furnace temperature = 1000°C) [Color figure can be viewed at wileyonlinelibrary.com]

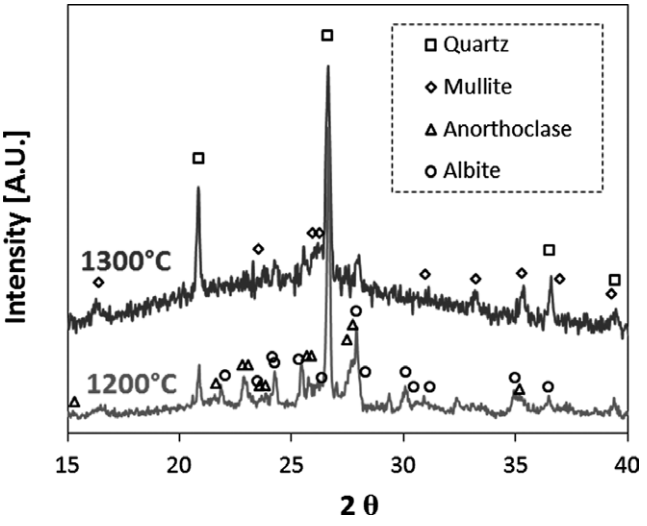

FIGURE 11 XRD patterns recorded on fast-fired sample treated at 1200 and 1300°C

findings already reported in flash sintering of glass-containing alumina.[17]

If we assume that glass viscosity at a given temperature is reduced by the electrical current application, this accounts for faster densification or more rapid swelling, depending on the sample temperature. If this is the case, it is clear why (as shown in Figure 9) flash sintering is more effective than fast firing at low temperature; and why, once the swelling temperature is reached, also the swelling process is accelerated during flash sintering.

The reasons behind such behavior are actually not clear, but they could be related to partial reduction in the material as a result of electrolytic reactions at the metal electrode/ceramic interface. The formation of partially reduced structures during flash sintering has been already discussed by Downs for YSZ[44]; Qin et al have also shown that the formation of nonstoichiometric ZrO_2 accounts for abnormal grain growth in the cathodic area during flash sintering.[45] According to the Ellingham diagram for ZrO_2 and SiO_2,[46] zirconium oxide is more stable than silica over the entire temperature range of interest here. Therefore, if a partial reduction in ZrO_2 upon flash sintering is possible, this can reasonably occur also for silica glass. In addition, the electric field can break the Na–O of K–O bonds leading to a structural rearrangement of the glassy phase. Under such hypothesis, different defects can be formed in the glass whose network is therefore partially fragmented,[47] this resulting in lower viscosity. Further analyses are clearly required for reaching a definitive conclusion.

4 | CONCLUSIONS

In this work, we have shown that flash sintering can be effectively applied to porcelain stoneware, expanding the application field of such technology to materials characterized by vitrification process upon sintering. The microstructural properties of the sintered specimens depend on the applied current and, at a furnace temperature of 1000°C, optimum densification is obtained with 14 mA/mm^2 in 30 seconds. Higher currents lead to swelling phenomena which are also observed during conventional sintering.

The obtained microstructures and the electrical behavior during flash sintering are directly linked to the vitrification process and to the decomposition of feldspars, as confirmed by XRD analysis.

Finally, we have shown that the densification obtained via flash sintering cannot be reproduced just by a very rapid heating.

ORCID

Mattia Biesuz http://orcid.org/0000-0002-4338-4177

REFERENCES

1. Cologna M, Rashkova B, Raj R. Flash sintering of nanograin zirconia in <5 s at 850°C. *J Am Ceram Soc*. 2010;93:3556-3559.
2. Downs JA, Sglavo VM. Electric field assisted sintering of cubic zirconia at 390°C. *J Am Ceram Soc*. 2013;96:1342-1344.
3. Yu M, Grasso S, Mckinnon R, et al. Review of flash sintering: materials mechanisms and modelling. *Adv Appl Ceram*. 2017;116:24-60.
4. Biesuz M, Luchi P, Quaranta A, et al. Theoretical and phenomenological analogies between flash sintering and dielectric breakdown in α-alumina. *J Appl Phys*. 2016;120:145107.
5. Muccillo R, Muccillo ENS. Light emission during electric field-assisted sintering of electroceramics. *J Eur Ceram Soc*. 2015;35:1653-1656.
6. Lebrun JM, Raj R. A first report of photoemission in experiments related to flash sintering. *J Am Ceram Soc*. 2014;97:2427-2430.
7. Steil MC, Marinha D, Aman Y, et al. From conventional AC flash-Sintering of YSZ to hyper-flash and double flash. *J Eur Ceram Soc*. 2013;33:2093-2101.
8. Muccillo R, Kleitz M, Muccillo ENS. Flash grain welding in yttria stabilized zirconia. *J Eur Ceram Soc*. 2011;31:1517-1521.
9. Hao X, Liu Y, Wang Z, et al. A novel sintering method to obtain fully dense gadolinia doped ceria by applying a direct current. *J Power Sources*. 2012;210:86-91.
10. Biesuz M, Dell'Agli G, Spiridigliozzi L, et al. Conventional and field-assisted sintering of nanosized Gd-doped ceria synthesized by co-precipitation. *Ceram Int*. 2016;42:11766-11771.
11. Gaur A, Sglavo VM. Densification of La0.6Sr0.4Co0.2Fe 0.8O3 ceramic by flash sintering at temperature less than 100 & #xB0; C. *J Mater Sci*. 2014;49:6321-6332.
12. Gaur A, Sglavo VM. Flash-sintering of $MnCo_2O_4$ and its relation to phase stability. *J Eur Ceram Soc*. 2014;34:2391-2400.
13. Prette ALG., Cologna M, Sglavo VM, et al. Flash-sintering of Co_2MnO_4 spinel for solid oxide fuel cell applications. *J Power Sources*. 2011;196:2061-2065.
14. Biesuz M, Sglavo VM. Flash sintering of alumina: effect of different operating conditions on densification. *J Eur Ceram Soc*. 2016;36:2535-2542.
15. Cologna M, Francis J, Raj R. Field assisted and flash sintering of alumina and its relationship to conductivity and MgO-doping. *J Eur Ceram Soc*. 2011;31:2827-2837.
16. McLaren C, Heffner W, Tessarollo R, et al. Electric field-induced softening of alkali silicate glasses. *Appl Phys Lett*. 2015;107:1-6.
17. Biesuz M, Sglavo VM. Liquid phase flash sintering in magnesia silicate glass-containing alumina. *J Eur Ceram Soc*. 2017;37:705-713.
18. Iqbal Y, Lee WE. Microstructural evolution in triaxial porcelain. *J Am Ceram Soc*. 2000;83:3121-3127.
19. Rahaman MN. *Ceramic Processing and Sintering*. New York, USA: Marcel Dekker; 1996.
20. Carter CB, Norton MG. Ceramic Materials Science and Engineering. 2007.
21. Lerdprom W, Chinnam RK, Jayaseelan DD, et al. Porcelain production by direct sintering. *J Eur Ceram Soc*. 2016;36:4319-4325.
22. Solids - Specific Heats, accessed on 4th July 2017, http://www.engineeringtoolbox.com/specific-heat-solids-d_154.htm.
23. Emissivity Coefficients of some common Materials, accessed on 4th July 2017, http://www.engineeringtoolbox.com/emissivity-coefficients-d_447.html

24. Leonard AJ. Structural analysis of the transition phases in the kaolinite- mullite thermal sequence. *J Am Ceram Soc*. 1977;60:37-43.
25. Sánchez-Soto PJ, de Haro MCJ, Pérez-Maqueda LA, et al. Effects of dry grinding on the structural changes of kaolinite powders. *J Am Ceram Soc*. 2000;83:1649-1657.
26. Xu X, Lao X, Wu J, et al. Microstructural evolution, phase transformation, and variations in physical properties of coal series kaolin powder compact during firing. *Appl Clay Sci*. 2015;115:76-86.
27. Boch JC, Niepce P. *Ceramic Materials*. Newport Beach, USA: ISTE; 2007.
28. Martín-Márquez J, Rincón JM, Romero M. Effect of firing temperature on sintering of porcelain stoneware tiles. *Ceram Int*. 2008;34:1867-1873.
29. Orts MJ, Escardino A, Amor JL, et al. Microstructural changes during the firing of stoneware floor tiles. *Appl Clay Sci*. 1993;8:193-205.
30. Francis J, Raj R. Influence of the field and the current limit on flash sintering at isothermal furnace temperatures. *J Am Ceram Soc*. 2013;96:2754-2758.
31. Todd RI, Zapata-Solvas E, Bonilla RS, et al. Electrical characteristics of flash sintering: thermal runaway of joule heating. *J Eur Ceram Soc*. 2015;35:1865-1877.
32. Zhang Y, Il Jung J, Luo J. Thermal runaway, flash sintering and asymmetrical microstructural development of ZnO and ZnO-Bi_2O_3 under direct currents. *Acta Mater*. 2015;94:87-100.
33. Dong Y, Chen IW. Onset criterion for flash sintering. *J Am Ceram Soc*. 2015;98:3624-3627.
34. Da Silva JGP, Al-Qureshi HA, Keil F, et al. A dynamic bifurcation criterion for thermal runaway during the flash sintering of ceramics. *J Eur Ceram Soc*. 2016;36:1261-1267.
35. Zhang Y, Nie J, Luo J. Effects of phase and doping on flash sintering of TiO_2. *J Ceram Soc Japan*. 2016;124:296-300.
36. Lee WE, Culver Y. Influence of mixing on mullite formation in porcelain. *J Eur Ceram Soc*. 2001;21:2583-2586.
37. Raj R. Joule heating during flash-sintering. *J Eur Ceram Soc*. 2012;32:2293-2301.
38. Grasso S, Sakka Y, Rrendtorff N, et al. Modeling of the temperature distribution of flash sintered zirconia. *J Ceram Soc Japan*. 2011;119:144-146.
39. Niu B, Zhang F, Zhang J, et al. Ultra-fast densification of boron carbide by flash spark plasma sintering. *Scr Mater*. 2016;116:127-130.
40. Ji W, Parker B, Falco S, et al. Ultra-fast firing: effect of heating rate on sintering of 3YSZ, with and without an electric field. *J Eur Ceram Soc*. 2017;37:2547-2551.
41. Zhang Y, Nie J, Chan JM, et al. Probing the densification mechanisms during flash sintering of ZnO. *Acta Mater*. 2017;125:465-475.
42. Todd RI. Flash sintering of ceramics: a short review. *Proc IV Adv Ceram Appl Conf*. 2017;1-12.
43. Lebrun JM, Jha SK, McCormack SJ, et al. Broadening of diffraction peak widths and temperature nonuniformity during flash experiments. *J Am Ceram Soc*. 2016;99:3429-3434.
44. Downs JA. *Mechanisms of Flash Sintering in Cubic Zirconia*. Trento:University of Trento, 2013.
45. Qin W, Majidi H, Yun J, et al. Electrode effects on microstructure formation during flash sintering of yttrium-stabilized zirconia. *J Am Ceram Soc*. 2016;99:2253-2259.
46. Barin I. *Thermochemical data of pure substances*. Weinheim: Federal Republic of Germany VCH; 1995.
47. Skuja L. Optically active oxygen-deficiency-related centers in amorphous silicon dioxide. *J Non Cryst Solids*. 1998;239:16-48.

How to cite this article: Biesuz M, Abate WD, Sglavo VM. Porcelain stoneware consolidation by flash sintering. *J Am Ceram Soc*. 2018;101:71–81. https://doi.org/10.1111/jace.15162

APPENDIX 1

The sample temperature evolution during fast firing was modeled as:

$$\Delta T_{S\,i} = \frac{\sigma \varepsilon S}{mC}\left(T_F^4 - T_S^4\right)\Delta t_i \qquad \text{(A1)}$$

where Δt_i (=0.01 second) is the integration time, S and m the sample surface and mass, respectively, C the specific heat of porcelain (=1000 J/kg K [22]), and $\Delta T_{s\,i}$ the specimen temperature variation within the integration time interval. The emissivity ε was assumed to be 0.93 [23] and 0.8. The sample temperature and time were then updated in the next interaction according to:

$$T_{S\,i+1} = T_{S\,i} + \Delta T_{S\,i} \qquad \text{(A2)}$$

$$t_{i+1} = t_i + \Delta t_i \qquad \text{(A3)}$$

where $\Delta T_{s\,i}$ and $\Delta T_{s\,i+1}$ are the specimen temperature at the beginning and at end of each integration interval. The initial sample temperature was assumed 27°C.